Scientific Research Publishing

Engineering, 2023, 15, 207-219
https://www.scirp.org/journal/eng
ISSN Online: 1947-394X
ISSN Print: 1947-3931

Study on the Law of Hydraulic Fracture Propagation in Low Permeability Thin Interbed Reservoir

YangJie Ou, Hao Liang

Hainan Branch of CNOOC (China) Limited, Haikou, China
Email: 1248541271@qq.com

How to cite this paper: Ou, Y.J. and Liang, H. (2023) Study on the Law of Hydraulic Fracture Propagation in Low Permeability Thin Interbed Reservoir. *Engineering*, **15**, 207-219.
https://doi.org/10.4236/eng.2023.154016

Received: February 13, 2023
Accepted: April 14, 2023
Published: April 17, 2023

Abstract

The third member of Weixinnanliu in the west of the South China Sea develops thin interbeds, and the vertical extension of fracturing fractures is excessive. Once the fractures extend vertically to the upper and lower aquifers, it is easy to cause water flooding of oil wells, and the effect after fracturing is not obvious. The present work aims to explore the longitudinal extension law of fractures in Low Permeability Thin Interbed Reservoir based on the finite element calculation platform. A three-dimensional expansion model of hydraulic fractures in the target reservoir was established, and the displacement, fracturing fluid viscosity, minimum horizontal principal stress difference, vertical stress, interlayer thickness, perforation point separation were studied. The interlayer distance and other factors affect the crack propagation law. The research results show that the thin interbed fractures have three forms: T-shaped fractures, through-layer fractures, and I-shaped fractures; for the target layer, the overlying stress is relatively large, and the minimum principal stress is along the horizontal direction. Vertical cracks; the farther the perforation point is or the greater the stress difference, the smaller the thickness of the interlayer required to control the fracture height; the stress difference is 3 MPa, and the distance between the perforation points exceeds 10 m, the thickness of the interlayer is required to be ≥4 m; In order to ensure that the width of the fracture in the middle spacer does not affect the placement of the proppant, it is recommended that the displacement be controlled within 3 m^3/min and the viscosity of the fracturing fluid is 150 mPa·s; in addition, the thickness of the spacer required to control the fracture height is different due to different geological parameters. Different, different wells need targeted analysis.

Keywords

Western South China Sea, Thin Interbed, Finite Element, Crack Propagation

1. Introduction

There are a large number of low porosity and permeability reserves in the west of the South China Sea, and it is difficult to achieve productivity breakthrough with conventional mining schemes [1] [2] [3]. The interbedding characteristics of reservoirs and barriers in Weixinan target block are significant, the longitudinal heterogeneity is strong, the compaction effect of deep reservoirs is serious, the brittleness ductility characteristics of reservoirs and barriers are unclear, and faults are developed, which may lead to problems such as limited longitudinal extension of fracturing fractures, difficulty in communicating multiple thin reservoirs up and down, and inability to form supporting fractures with high conductivity [4] [5]. For thin interbedding fracturing, once the fractures break through the gas cap or aquifer, it will cause serious water and gas outflow from the well. At the same time, for the target block, it is necessary to extend the cracks within the preferred horizon as much as possible to increase the reconstruction strength of the preferred horizon [6].

In view of the vertical extension of hydraulic fractures in multi lithologic layered reservoirs, scholars have conducted a lot of research. Influenced by interlayer rock properties, principal stress conditions, interface properties and construction parameters, hydraulic fractures show different shapes. Ahmed and Newberry [7] qualitatively put forward the hydraulic fracturing reconstruction design method and perforation layout technology for wells with multiple production layers. Ben Naceur and Roegiers [8] quantitatively deduced for the first time the mathematical model of multi fracture propagation for simultaneous hydraulic fracturing of multiple pay zones. Li Yang *et al.* [9] [10] established a multi-layer hydraulic fracture propagation model by using finite element method, and studied the vertical fracture propagation law under different interlayer permeability and rock mechanical properties. Huang *et al.* [11] used 3D lattice model to simulate hydraulic fracturing, and analyzed the impact of different perforation positions on the initiation and expansion of fractures near the wellbore. Zhao Haifeng *et al.* [12] comprehensively described the possible expansion or crack arrest behavior when the hydraulic fracture intersects the stratum interface from the perspective of rock fracture mechanics, and gave the corresponding judgment basis. Based on the physical model experiment of true triaxial hydraulic fracturing, Hou *et al.* [13] [14] [15] [16]

To sum up, although much research has been carried out on multi-layer fracturing, they are mainly focused on the fracture propagation law of single lithology or homogeneous layered reservoirs in each layer. The numerical models are mostly simplified into two-dimensional problems, ignoring the competitive propagation process of fracture length and fracture height, or ignoring the influence of lithologic interfaces, resulting in the calculated fracture height being much higher than the actual fracture height. In this paper, based on the actual geological characteristics of Weixinan reservoir, a three-dimensional finite element model of hydraulic fracture propagation is established, and the effects of

interlayer physical property difference, principal stress conditions, perforation point location, spacer thickness and fracturing operation parameters on the hydraulic fracture propagation law are studied, so as to provide guidance for the integrated fracturing of offshore low-permeability thin interbeds.

2. Geological Characteristics of Reservoir

Through early drilling, it is found that the oil and gas display of the third member of Weixinliu Formation reaches 135 m, with a depth of about 3000 m. Thin oil layers are relatively developed, with a layer thickness of 1 to 3 m. The interlayer is usually red brown mudstone without water. The average porosity of oil reservoir is 13.37% according to logging interpretation, and the permeability is mainly distributed in 0.1×10^{-3} - 10×10^{-3} μm^2, which is a low porosity and low permeability/ultra-low permeability reservoir with poor overall physical properties. Through image analysis and laser particle size analysis, the average pore diameter of Liusan Member rocks is 56.2 - 280 μm. The average throat value is 22 - 42 μm. The median particle size is 0.04 - 0.23 μm. Formation heterogeneity is relatively strong at different depths. Through casting thin section and scanning electron microscope experiments, the main reservoir space types of Liusan Member rocks are intergranular pores, intergranular dissolved pores, intragranular dissolved pores, and a small number of cracks are also seen. The cracks are mainly intergranular cracks, as shown in Figure 1. In general, the lithology of the longitudinal profile of the target reservoir changes complicatedly, and the rock mechanical properties and principal stress conditions differ greatly. The maximum interlayer stress difference can reach 7 MPa. Compared with the traditional layered sand shale reservoir, the complex stratigraphic environment and principal stress state of the target reservoir greatly improve the difficulty of hydraulic fracturing.

3. Mathematical Model

3.1. Governing Equation

3.1.1. Fluid Structure Coupling Equation

In order to simplify the mathematical model calculation, the composition and structure of rock are divided into two parts: solid skeleton and pores between

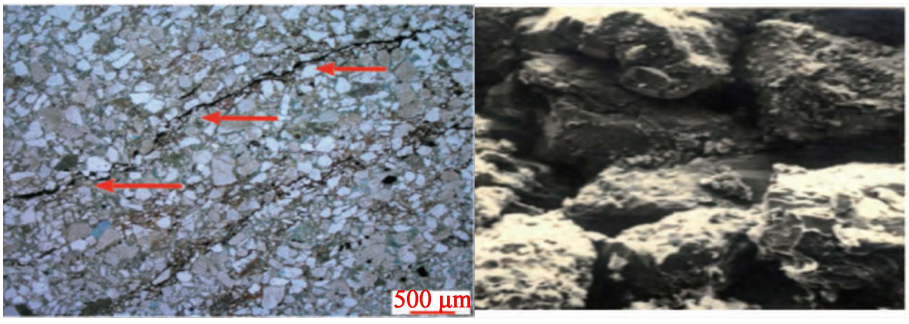

Figure 1. Thin sections of core casting and sem images.

skeletons. The equilibrium equation of rock solid skeleton deformation mechanics is [17]

$$\int_V (\sigma - p_w I)\delta\varepsilon \mathrm{d}V = \int_S t\delta v \mathrm{d}S + \int_V f\delta v \mathrm{d}V \tag{1-1}$$

where V is volume, m^3, σ is the total stress, Pa. p_w is the wetting phase pressure, Pa. I s the identity matrix, δ is Cronek symbol. S is the area, m^2, ε is the virtual strain rate, s^{-1}. t Is the surface force vector, N/m^2. v Is the virtual velocity vector. f Is the physical force vector, N/m^3.

The continuity equation of fluid seepage is

$$\int_V \frac{1}{J}\frac{\partial}{\partial t} J\rho_w n_w \mathrm{d}V + \int_V \frac{\partial}{\partial X}\rho_w n_w v_w \mathrm{d}V = 0 \tag{1-2}$$

where, J is the volume change ratio. p_w is the fluid density, kg/m^3. n_w Is porosity. X is the space vector, m/s. v_w Is the fluid seepage velocity, m/s. It is assumed that the fluid flow in the rock satisfies Darcy's law:

$$v_w = -\frac{1}{n_w g \rho_w} k\left(\frac{\partial p_w}{\partial X} - \rho_w g\right) \tag{1-3}$$

Where g is the acceleration of gravity, m/s^2. k Is the velocity vector of rock seepage, m/s.

3.1.2. Hydraulic Fracture Initiation and Propagation Criterion

Cohesion method is to characterize the initial damage and evolution process of viscous element through the traction separation law, that is, to simulate the initiation and propagation process of hydraulic cracks [18] [19] (see **Figure 2**. In the figure, T is the stress, T_0 is the stress at the initial damage of viscous element, μ_0 is the displacement of viscous element at initial damage, μ_M is the maximum displacement during the expansion of viscous element, and d is the opening distance of viscous element surface).

The maximum strain criterion is used to judge whether the initial damage occurs to the viscous element. When the strain in any direction reaches its critical

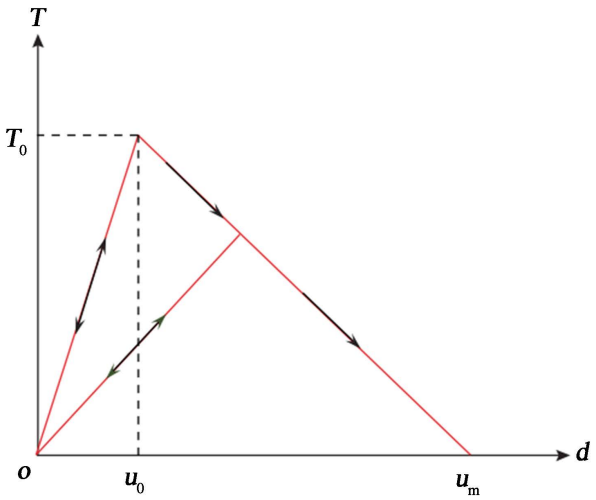

Figure 2. Crack initiation and propagation criteria for viscous elements.

strain, the cohesive starts to produce damage:

$$\max\left\{\frac{\langle\varepsilon_n\rangle}{\varepsilon_n^o},\frac{\varepsilon_s}{\varepsilon_s^o},\frac{\varepsilon_t}{\varepsilon_t^o}\right\}=1 \tag{1-4}$$

where ε_n^o —normal critical strain of cohesive element, dimensionless;

ε_s^o, ε_t^o —critical strains in two shear directions, dimensionless.

3.1.3. Fluid Flow Equation in Fracture

As shown in Figure 3, during fracturing fluid injection, the flow process in the fracture includes tangential flow along the fracture extension direction and normal flow perpendicular to the fracture surface. This study describes that the tangential flow of fracturing fluid in hydraulic fractures is incompressible Newtonian fluid flow

$$q=\frac{w^3}{12\mu}\Delta p \tag{1-5}$$

where, q is fluid flow in hydraulic fractures, m^3/s; w is the width of hydraulic fracture, m. μ is the fluid viscosity, Pa·s; Δp is the fluid pressure gradient along the extension direction of hydraulic fracture, Pa/m.

The fracturing fluid filtration behavior can be described as

$$\begin{aligned} q_t &= C_t\left(P_i-P_t\right)\\ q_b &= C_b\left(P_i-P_b\right)\end{aligned} \tag{1-6}$$

where, q_t, q_b are respectively the flow of unit time and unit area on the upper and lower surfaces of hydraulic fractures, m^3/s. C_t, C_b is the filtration coefficient of the upper and lower surfaces of the hydraulic fracture, m/(Pa·s). P_t, P_b Pore pressure on the upper and lower surfaces of hydraulic fractures, Pa. P_i Is the fluid pressure in the hydraulic fracture, Pa.

3.2. Modelling

Taking Well A in Weixinan target block as an example well, the reservoir of the fracturing horizon is sand mud alternating layer, the red well section is sandstone layer, and the rest of the well sections are mudstone layer, with thin sand

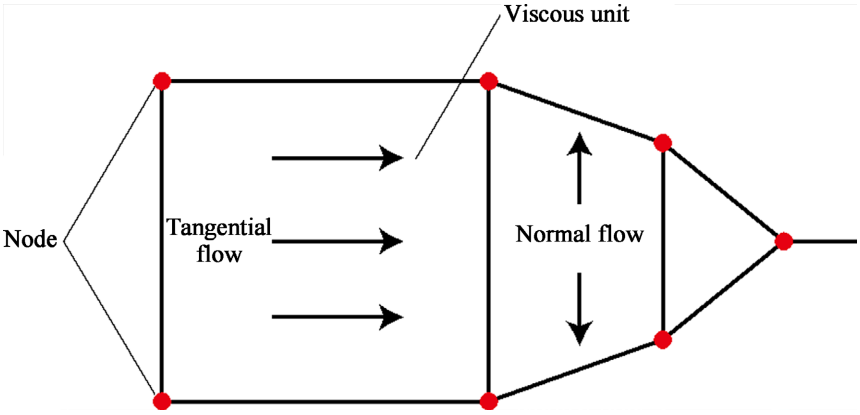

Figure 3. Schematic diagram of fluid flow in hydraulic fracture.

mud alternating deposition, as shown in Figure 4(a). According to the distribution and thickness proportion of reservoir barriers, a three-dimensional finite element model of dynamic fracture expansion is established. The model is 50 m long, 40 m wide and 15.5 m high, with 4 barriers and 4 reservoirs in total.

According to the geometric model, the three-dimensional finite element model is established. The model includes 138,804 nodes and 94,939 units in total. Among them, the type of simulated wellbore unit used is pipe unit (FP3D2), and the type of simulated formation matrix unit is pore pressure unit (C3D8P) and simulated fracture unit pore pressure cohesion unit (COH3D8P). The cross grid of weak interface and vertical hydraulic fracture of sand mud interbed is shown in Figure 4(b). The stress loading mode and boundary condition setting are similar to the crack propagation of 3D single thick sandstone.

4. Simulation Results and Analysis

4.1. Variable Displacement Simulation

When the injection rate of fracturing fluid is 1 m^3/min, or 2 m^3/min, or 3 m^3/min, or 4 m^3/min, or 5 m^3/min, we study the process from formation initiation to fracture propagation. Under the condition of constant total injection amount, the fracture length decreases and the fracture height increases with the increase of the displacement, and the upper and lower barriers are penetrated near the perforation point, as shown in Figure 5; under the condition of constant total injection amount, the maximum width of the fracture in the fracturing layer gradually increases with the increase of the displacement. When the displacement is 5 m^3/min, the maximum width of the fracture is 4.497 mm, but the width of the fracture in the interlayer will decrease, as shown in Figure 6. When the displacement exceeds 3 m^3/min, the crack propagation slows down. Therefore, in order to ensure that the width of the cracks in the interlayer does not affect the placement of the proppant, combined with the offshore operation conditions, it is recommended that the displacement be controlled within 3 m^3/min.

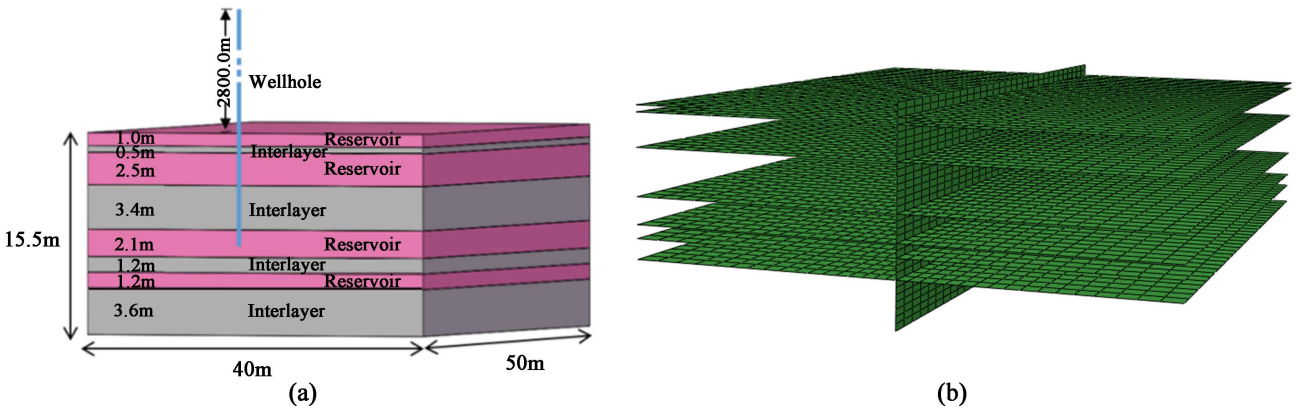

Figure 4. Schematic diagram of model establishment. (a) 3DHydraulic fracture propagation model; (b) Preset viscous element surface.

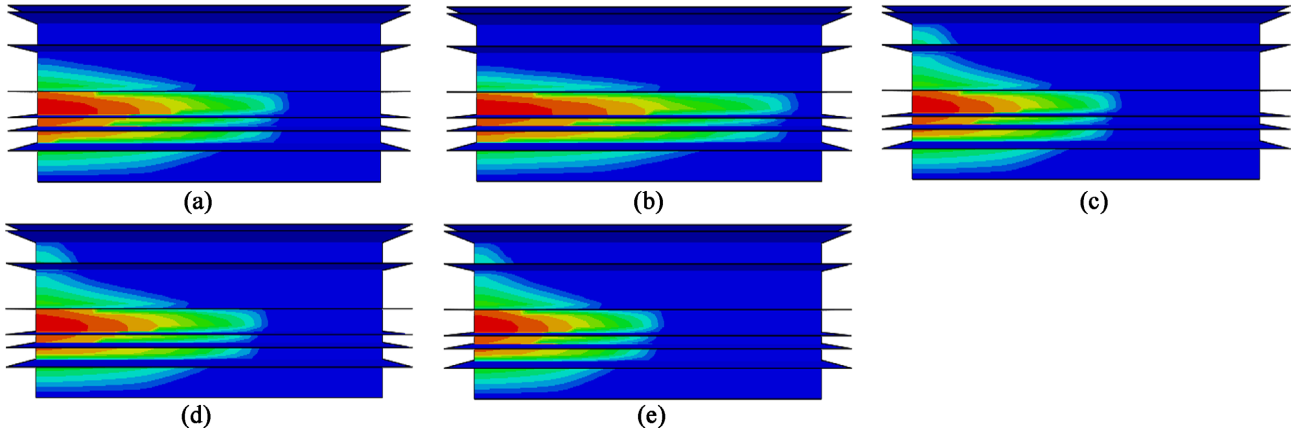

Figure 5. The law of crack propagation with different displacement. (a) 1 m^3/min Crack propagation; (b) 2 m^3/min Crack propagation; (c) 3 m^3/min Crack propagation; (d) 4 m^3/min Crack propagation; (e) 5 m^3/min Crack propagation.

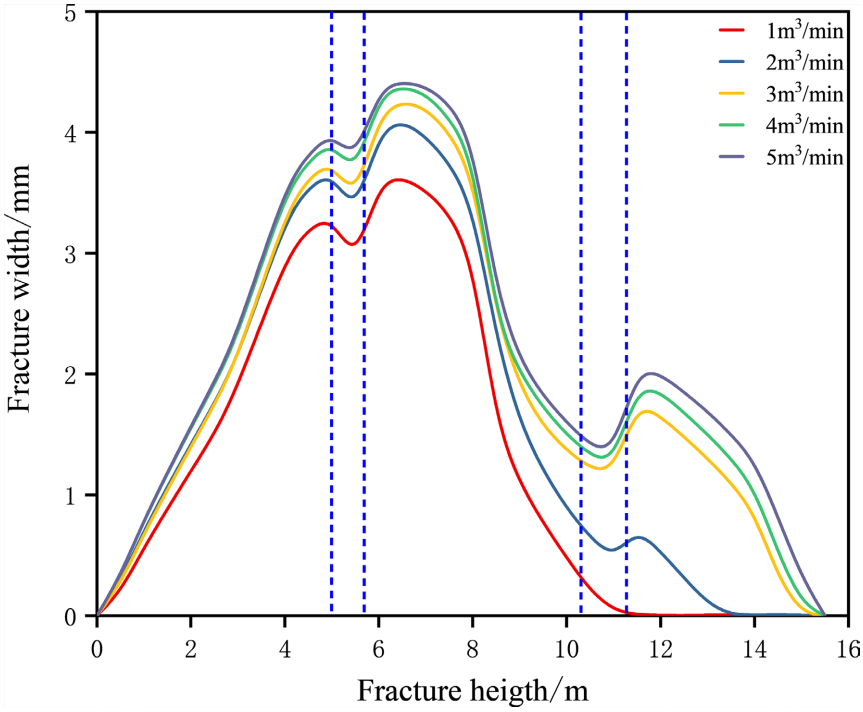

Figure 6. Trend diagram of fracture parameters changing with displacement.

4.2. Simulation of Variable Pressure Fracturing Fluid Viscosity

When the construction displacement is 2 m^3/min, and the viscosity is 50 mpa·s, or 100 mpa·s, or 150 mpa·s, or 200 mpa·s, or 250 mpa·s, we study the fracture propagation under these five different conditions. The influence of the interlayer on the crack width decreases with the increase of viscosity. The influence of the interlayer on the crack growth morphology can be reduced by appropriately increasing the viscosity, as shown in Figure 7. When the viscosity exceeds 150 mPa·s, the fracture parameters change slowly.

The greater the viscosity of the crosslinked fracturing fluid, the stronger the ability to create fractures for reservoir rocks, and the greater the viscosity of the

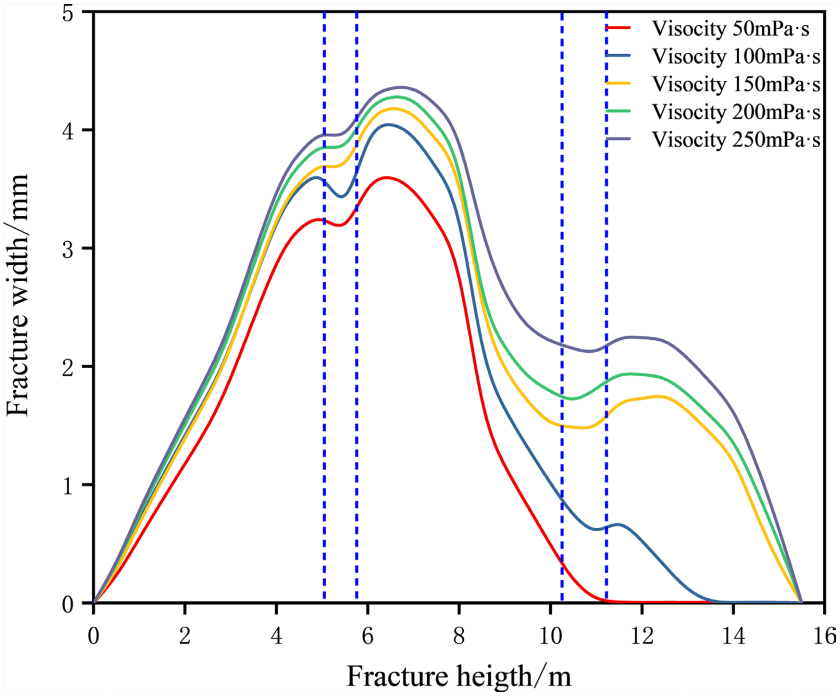

Figure 7. Trend diagram of fracture parameters changing with viscosity.

fracturing fluid, the smaller the filtration, which makes the longitudinal extension height and width of the artificial fractures larger. Therefore, the fracturing fluid should not only carry sand normally, but also reduce the viscosity of fracturing fluid as much as possible.

4.3. Simulation of Variable Minimum Horizontal Principal Stress Difference

When the construction displacement is 2 m^3/min and the minimum horizontal principal stress difference between the upper and lower interlayers is 0 MPa, or 2 MPa, or 4 MPa, or 6 MPa, or 8 MPa, we study the fracture propagation under these five different conditions. When the minimum horizontal principal stress difference exceeds 6 MPa, the interlayer can effectively prevent the longitudinal expansion of the crack. As shown in **Figure 8**, the greater the difference in geo-stress, the smaller the overall height of the crack. This is because the fluid pressure must overcome the geo-stress to make the fracture expand, so the geo-stress is a hindrance to the fracture extension. The high stress makes the fracture height smaller, while the width increases, and the fracture opens more in the pay stratum. For the stratum with only one pay stratum, this is the desired situation in engineering practice.

4.4. Simulation of Variable Vertical Stress

When the construction displacement is 2 m^3/min, and the vertical stress of the interlayers is 40 MPa, or 44 MPa, or 48 MPa, or 52 MPa, or 56 MPa, we study the fracture propagation under these five conditions. As shown in **Figure 9**, when

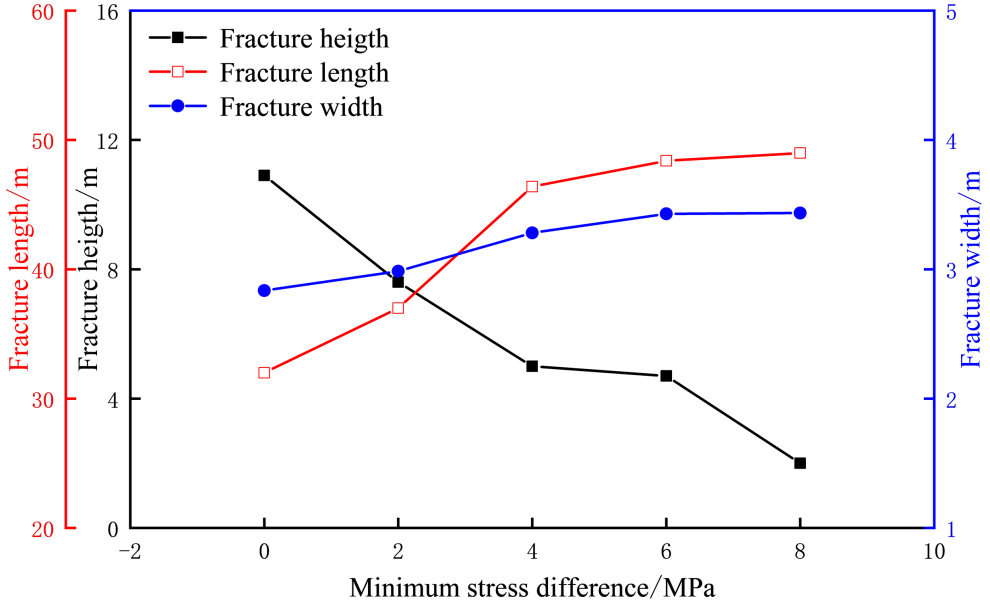

Figure 8. Trend diagram of fracture parameters changing with minimum stress difference.

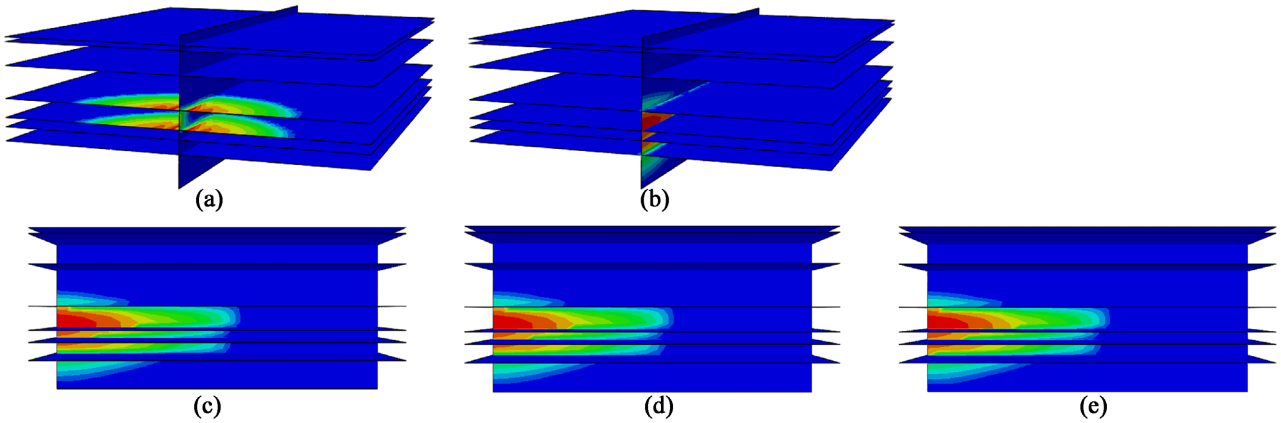

Figure 9. The law of crack propagation with different vertical stresses. (a) 40 MPa; (b) 44 MPa; (c) 48 MPa; (d) 52 MPa; (e) 56 MPa.

the vertical stress is 40 MPa, it is less than the minimum horizontal principal stress of 42 MPa. At this time, the crack extends at the horizontal interface between the upper and lower interlayer. When the vertical ground stress is greater than the minimum horizontal stress, the crack extends vertically. For the target horizon in Weixinan, the burial depth is large, and the overlying stress is large. Generally speaking, the minimum principal stress in this case is along the horizontal direction, and vertical fractures are formed by fracturing.

4.5. Simulation of Variable Interlayer Thickness

When the construction displacement is 3 m^3/min, and the thickness of the upper interlayer is 3 m, or 4 m, or 5 m, or 6 m, or 7 m, we study the fracture propagation under these five conditions. Taking the reservoir thickness of 2 m as an example, the fracture height decreases with the increase of the interlayer thick-

ness; When the minimum horizontal principal stress difference of the reservoir interlayer is 3 MPa and 5 MPa respectively, when the thickness of the interlayer is greater than 6.0 m and 5.0 m respectively, the extension of the artificial fracture in the longitudinal direction can be effectively shielded, as shown in Figure 10.

4.6. Simulation of Distance between Variable Perforation Point and Interlayer

When the construction displacement is 3 m^3/min, the stress difference between reservoir and interlayer is 3 MPa, or 5 MPa, and the distance between the perforating point and the interlayer is 2.7 m, or 4.9 m, or 7.0 m, or 8.6 m, or 10.7 m, or 13.2 m, we study the fracture propagation under these different conditions. The fracture propagation is calculated when the perforation point is 2.7 m, 4.9 m, 7.0 m, 8.6 m, 10.7 m and 13.2 m away from the interlayer. The results show that the farther the perforation point is or the greater the stress difference is, the

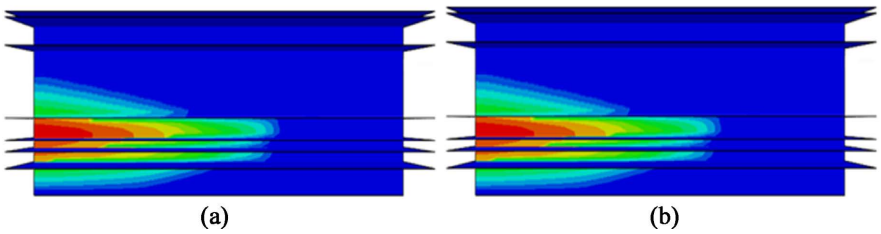

Figure 10. The law of crack propagation with different thickness of interlayer and minimum horizontal principal stress difference. (a) 6 m crack propagation of interlayer (stress difference 3 MPa); (b) Crack propagation at 5 m interval (stress difference 5 MPa).

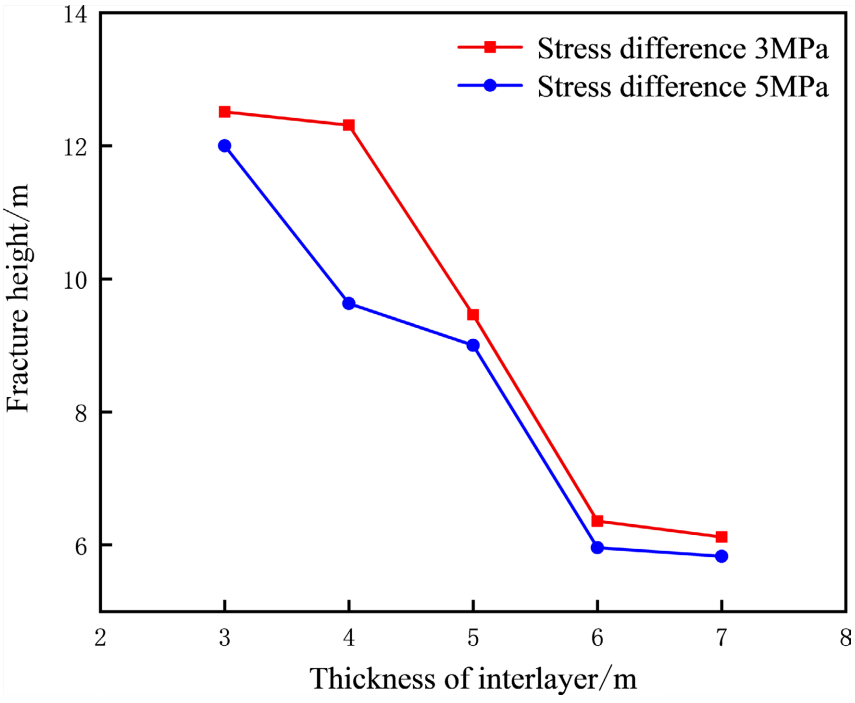

Figure 11. Trend diagram of fracture parameters changing with thickness of interlayer.

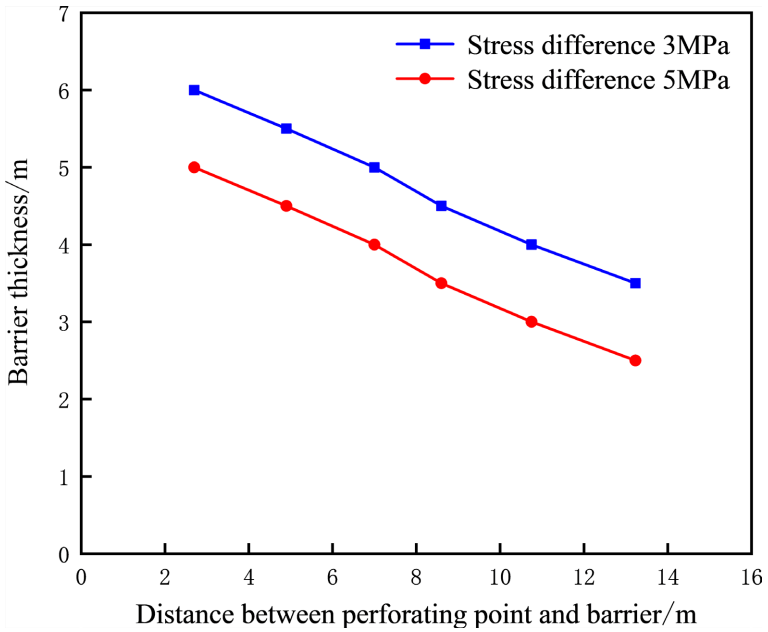

Figure 12. Trend diagram of barrier thickness changing with the distance between perforating point and barrier.

smaller the thickness of the spacer required for controlling the joint height is; The stress difference is 3 MPa, the perforation point distance is more than 10 m, and the thickness of the interlayer is required to be ≥4 m; The stress difference is 5 MPa, the perforation point distance is more than 10 m, and the thickness of the interlayer is required to be ≥3 m; For the barrier that does not conform to the stress difference and the distance between perforation points, the artificial diaphragm technology can be used to improve the stress difference of the reservoir barrier and control the fracture height.

5. Conclusion

1) The crack propagation of thin interbed presents three types: T-shaped joint, cross layer joint and I-shaped joint; for the target layer, the overburden stress is large, the minimum principal stress is along the horizontal direction, and the fracturing generally forms a vertical fracture; The numerical simulation results of thin interbed fracture propagation show that the main controlling factors of fracture height are horizontal geo-stress difference, thickness of interlayer, fracturing fluid displacement and viscosity.

2) The fracture width will suddenly decrease at the interlayer. To ensure that the width of the interlayer fracture does not affect the proppant placement, it is recommended that the displacement be controlled within 3 m^3/min, and the viscosity of the fracturing fluid be 150 mPa·s.

3) For the target layer in the third section of Weizhouliu, the farther the perforation point is or the greater the stress difference is, the smaller the thickness of the spacer required for controlling the fracture height is; The stress difference is 3 MPa, the perforation point distance is more than 10 m, and the thickness of

the interlayer is required to be ≥4 m; In addition, due to different geological parameters, the thickness of the interlayer required for controlling the fracture height is different, and specific analysis is required for different wells.

Conflicts of Interest

The authors declare no conflicts of interest regarding the publication of this paper.

References

[1] Xie, Y.H. (2018) Exploration and Practice of Low Permeability Reservoirs Exploration and Development in Western South China Sea. *China Offshore Oil and Gas*, **30**, 80-85.

[2] Tang, B., Tang, Z.J., Geng, Y.C., *et al.* (2013) Drilling and Completion Technologies for Efficient Exploitation of Low-Permeability Oil and Gas Fields in China: A State-of-the-Art Review. *Natural Gas Industry*, **33**, 65-70.

[3] Wu, B.L., Yang, K., Cheng, Y.X., *et al.* (2021) Experimental Study of Proppant Conductivity in Low Permeability Reservoir in the South China Sea. *Petroleum Drilling Techniques*, **49**, 86-92.

[4] Lei, H., Ma, Y.X., Zhang, H., *et al.* (2017) Effect of Water Sensitivity on Oil-Water Flow Characterisitics and Its Mechanism for WS 17-2 Low-Permeability Glutenite Reservoir. *Complex Hydrocarbon Reservoirs*, **10**, 55-59.

[5] Li, L., Hu, W.L., Luo, Q.Y., *et al.* (2021) Inpact of Non-Darcy Seepage Effect on the Productivity of Low Permeability Reservoirs in South China Sea. *Petroleum Geology & Oilfield Development in Daqing*, **40**, 160-167.

[6] Bian, X.B., Zhang, S.C., Han, X.L., *et al.* (2011) Adaptability Evaluation on Hydraulic Fracturing Technology of Offshore Low Permeability Reservoirs. *Science Technology and Engineering*, **11**, 1671-1815.

[7] Ahmed, U., Newberry, B.M. and Cannon, D.E. (1985) Hydraulic Fracture Treatment Design of Wells with Multiple Zones. Society of Petroleum Engineers. *SPE/DOE Low Permeability Gas Reservoirs Symposium*, Denver, 19 May 1985, SPE-13857-MS. https://doi.org/10.2118/13857-MS

[8] Ben-Naceur, K. and Roegiers, J. (1990) Design of Fracturing Treatments in Multilayered Formations. *SPE Production Engineering*, **5**, 21-26. https://doi.org/10.2118/17712-PA

[9] Li, Y., Deng, J.G., Liu, W., *et al.* (2017) Numerical Simulation of Limited Entry Technique in Multi-Stage and Multi-Cluster Horizontal Well Fracturing. *Fault-Block Oil & Gas Field*, **24**, 69-73.

[10] Guo, J., Luo, B., Lu, C., *et al.* (2017) Numerical Investigation of Hydraulic Fracture Propagation in a Layered Reservoir Using the Cohesive Zone Method. *Engineering Fracture Mechanics*, **186**, 195-207. https://doi.org/10.1016/j.engfracmech.2017.10.013

[11] Huang, L.K., Liu, J.J., Zhang, F.S., *et al.* (2020) 3D Lattice Modeling of Hydraulic Fracture Initiation and Near-Wellbore Propagation for Different Perforation Models. *Journal of Petroleum Science and Engineering*, **191**, Article 107169. https://doi.org/10.1016/j.petrol.2020.107169

[12] Zhao, H.F., Cheng, M. and Jin, Y. (2009) Extending Behavior of Hydraulic Fracture on Formation Interface. *Acta Petrolei Sinica*, **30**, 450-454.

[13] Hou, B., Chang, Z., Fu, W.N., *et al.* (2019) Fracture Initiation and Propagation in a Deep Shale Gas Reservoir Subject to an Alternating Fluid-Injection Hydraulic-Fracturing Treatment. *SPE Journal*, **24**, 1839-1855. https://doi.org/10.2118/195571-PA

[14] Wan, L.M., Hou, B., Tan, P., *et al.* (2019) Observing the Effects of Transition Zone Properties on Fracture Vertical Propagation Behavior for Coal Measure Strata. *Journal of Structural*, **126**, 69-82. https://doi.org/10.1016/j.jsg.2019.05.005

[15] Tan, P., Jin, Y., Han, K., *et al.* (2017) Vertical Propagation Behavior of Hydraulic Fractures in Coal Measure Strata Based on True Triaxial Experiment. *Journal of Petroleum Science and Engineering*, **158**, 398-407. https://doi.org/10.1016/j.petrol.2017.08.076

[16] Tan, P., Jin, Y., Yuan, L., *et al.* (2019) Understanding Hydraulic Fracture Propagation Behavior in Tight Sandstone-Coal Interbedded Formations: An Experimental Investigation. *Petroleum Science*, **16**, 148-160. https://doi.org/10.1007/s12182-018-0297-z

[17] Fu, S.H., Cheng, M., Xiao, Y., *et al.* (2021) Law of Hydraulic Fracture Propagation in Coal Measure Shale Reservoir. *Fault-Block Oil & Gas Field*, **28**, 555-560.

[18] Zhu, H.Y., Zhao, J., Deng, J.G., *et al.* (2013) Numerical Simulation on Micro-Annulus Initiation and Propagation during Hydraulic Fracturing. *Computer Aided Engineering*, **22**, 443-447.

[19] Zhu, H.Y., Tao, L., Liu, D.Q., *et al.* (2018) Fracability Estimation for Longmaxi Shale: Coupled Brittleness, Stress-Strain and Fracture. *Arabian Journal for Science and Engineering*, **43**, 6639-6652. https://doi.org/10.1007/s13369-018-3422-9